Isolated theta waves originating from the midline thalamus trigger memory reactivation during NREM sleep in mice

Qin Xiao, Minmin Lu, Xiaolong Zhang, Jiangheng Guan, Xin Li, Ruyi Wen, Na Wang, Ling Qian, Yixiang Liao, Zehui Zhang, Xiang Liao, Chenggang Jiang, Faguo Yue, Shuancheng Ren, Jianxia Xia, Jun Hu, Fenlan Luo, Zhian Hu, Chao He

Supplementary Information

Supplementary information contains 14 supplementary figures

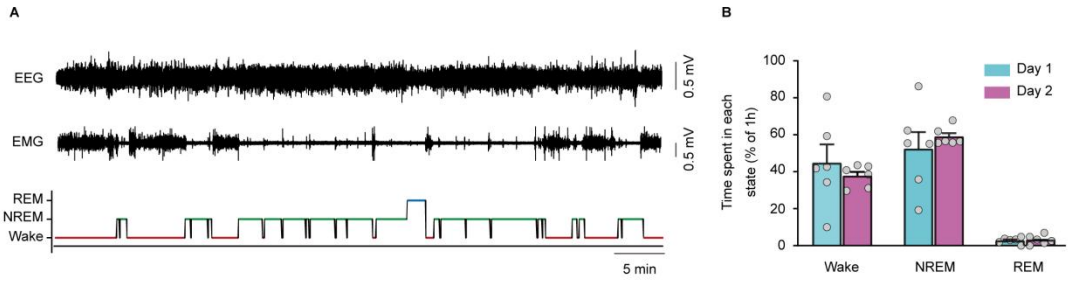

Supplementary Figure 1. Sleep-wakefulness architecture during post-training phase.

A Representative raw EEG-EMG traces, and corresponding color-coded hypnogram during post-training phase.

B Comparison of the time spent in each state during post-training phase on the first day and the second day. White circles represent individual mouse (Two tailed unpaired *t* test, n = 6 mice for each group, day 1-wake vs. day 2-wake, $t_{10} = 0.700$, $P = 0.500$; day 1-NREM vs. day 2-NREM, $t_{10} = -0.695$, $P = 0.503$; day 1-REM vs. day 2-REM, $t_{10} = -0.303$, $P = 0.768$).

n = 6 mice were shared in the experiment of recording spikes and LFP in the MEC as well as EEG-EMG recording in the Fig. 1 and Supplementary Figure. 1-3.

Data are presented as mean ± s.e.m. Source data are provided as a Source Data file.

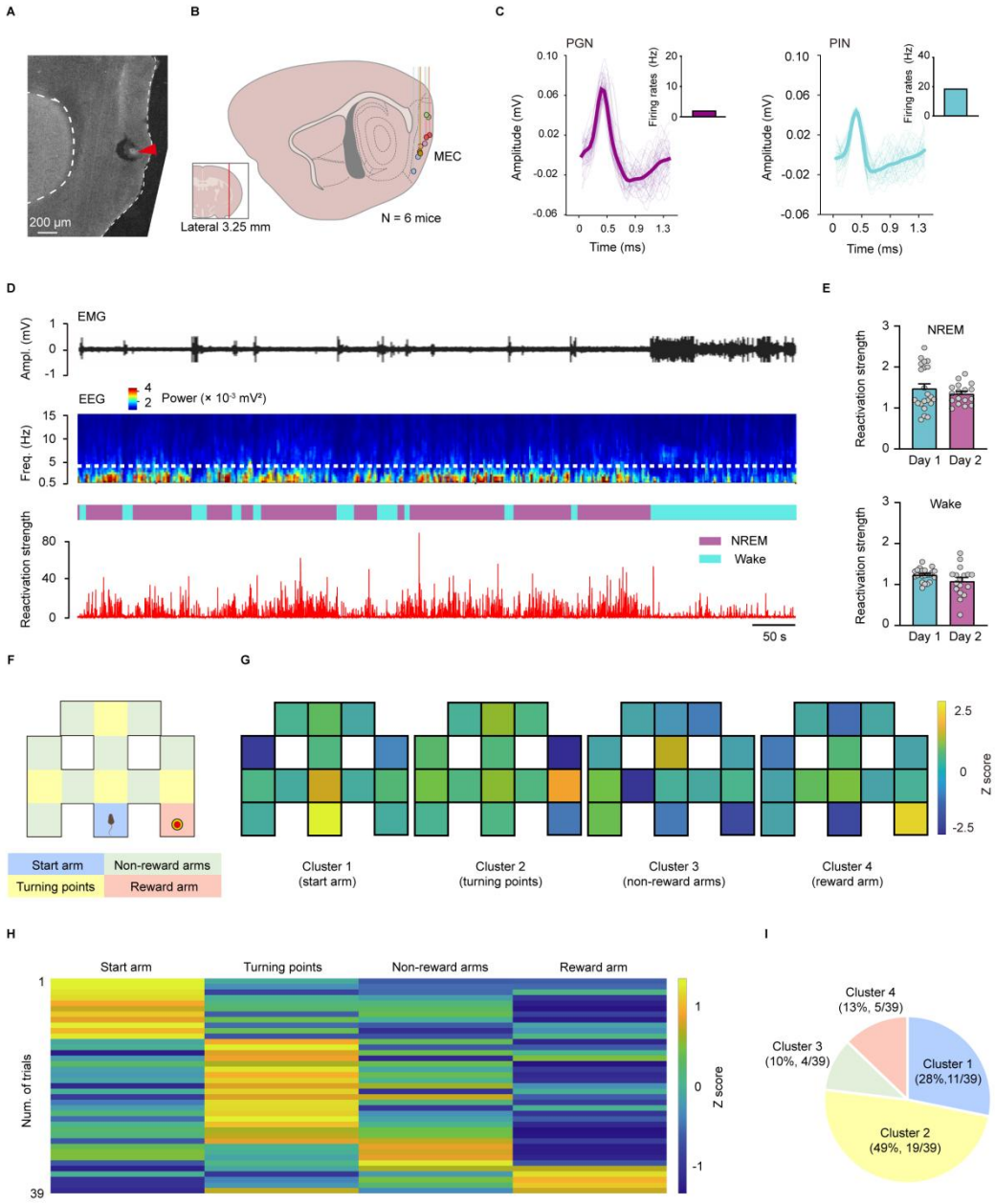

Supplementary Figure 2. Firing patterns of MEC assemblies representing spatial memory reactivate during post-training NREM sleep.

A Representative images showing the electrode (red arrowhead) implanted in the MEC.

B Recording sites were depicted as colored circles for all tested mice (n = 6 mice).

C Characteristic of the spike waveforms of a putative glutamatergic neuron (PGN, left)

or putative interneuron (PIN, right) in the MEC. Insets show the firing rate of an example PGN or PIN.

D Representative raw EMG traces, EEG power spectrum, color-coded hypnogram, and reactivation strength during post-training phase. Ampl., amplitude. Freq., frequency.

E Comparison of reactivation strength during day 1 and day 2 post-training NREM sleep (top) and wakefulness (bottom). Data are presented as mean ± s.e.m. (Welch's t-test, day 1: n = 22, day 2: n = 17, NREM: $t_{37} = 1.002$, $P = 0.324$; wake: $t_{37} = 1.629$, $P = 0.118$).

F Diagram showing the space of maze was divided into four sections: start arm (blue); non-reward arm (green); turning points (yellow); reward arm (bright pink). Red circle represents the food as a reward.

G Schematic showing the spatial distribution of four typical PC in the maze. The PC characterizes the firing pattern during training phase.

H Heatmap showing the spatial distribution of the PC in the maze.

I Pie chart showing the ratio of four types of space-related firing patterns.

Data are presented as mean ± s.e.m. Source data are provided as a Source Data file.

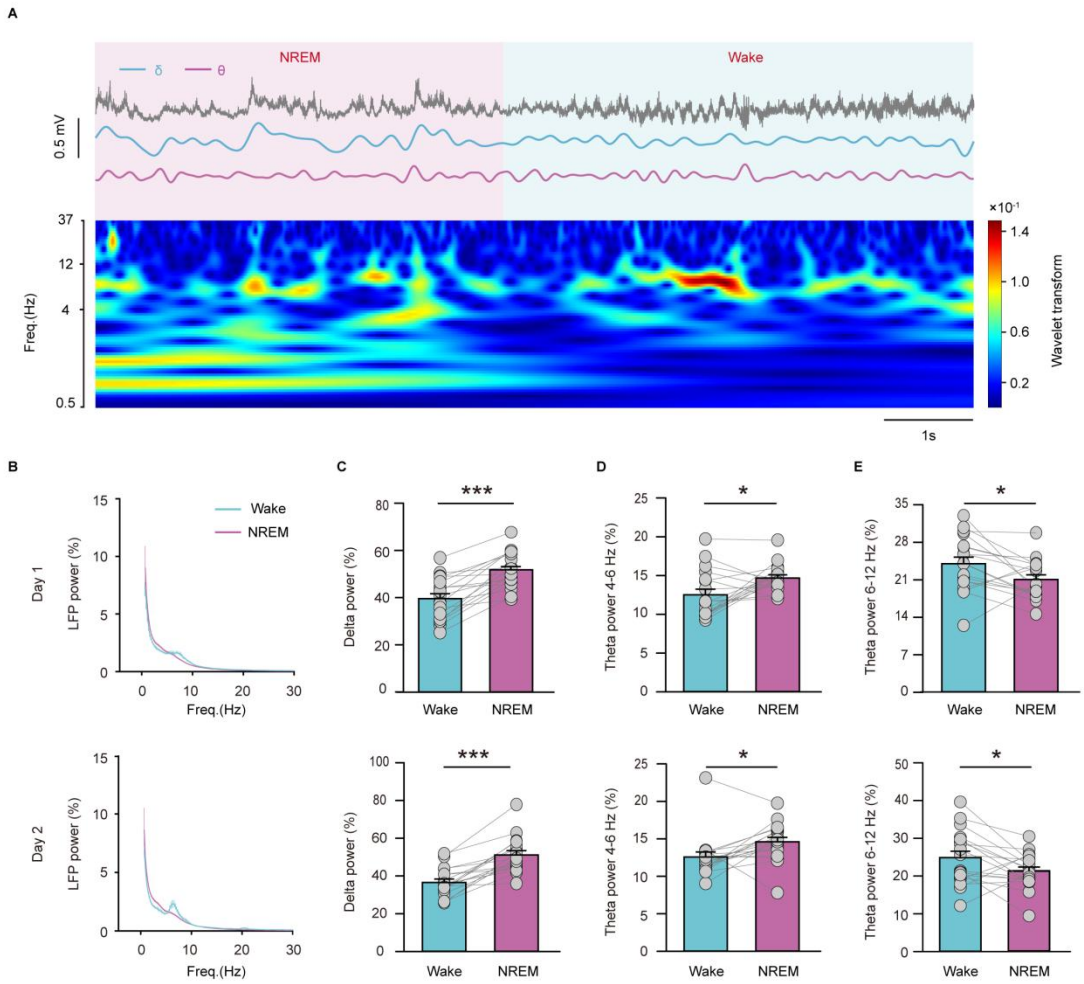

Supplementary Figure 3. Characteristic of oscillatory activities of the MEC during NREM sleep-wakefulness transitions.

A Raw LFP (Gray: raw trace; cyan: filtered delta; magenta: filtered theta) and corresponding power spectrum during post-training NREM sleep and wakefulness.

B Diagram showing normalized LFP power in different bands during day 1 and day 2 post-training NREM sleep and wakefulness.

C, D, E Changes in the delta power (**C**), 4-6 Hz theta power (**D**) and 6-12 Hz theta power (**E**) in the MEC during post-training NREM sleep and wakefulness (Two tailed paired *t* test, n = 18 channels, Day 1-delta: t_{17} = -6.356, $P = 7.18\times10^{-6}$; day 2-delta: t_{17} = -7.068, $P = 1.89\times10^{-6}$; day 1-low theta: t_{17} = -2.749, P = 0.0137; day 2-low theta:

t_{17} = -2.788, P = 0.0126; day 1-high theta: t_{17} = 2.433, P = 0.0263; day 2-high theta: t_{17} = 2.203, P = 0.0417).

*P < 0.05, ***P < 0.001. Data are presented as mean ± s.e.m. Source data are provided as a Source Data file.

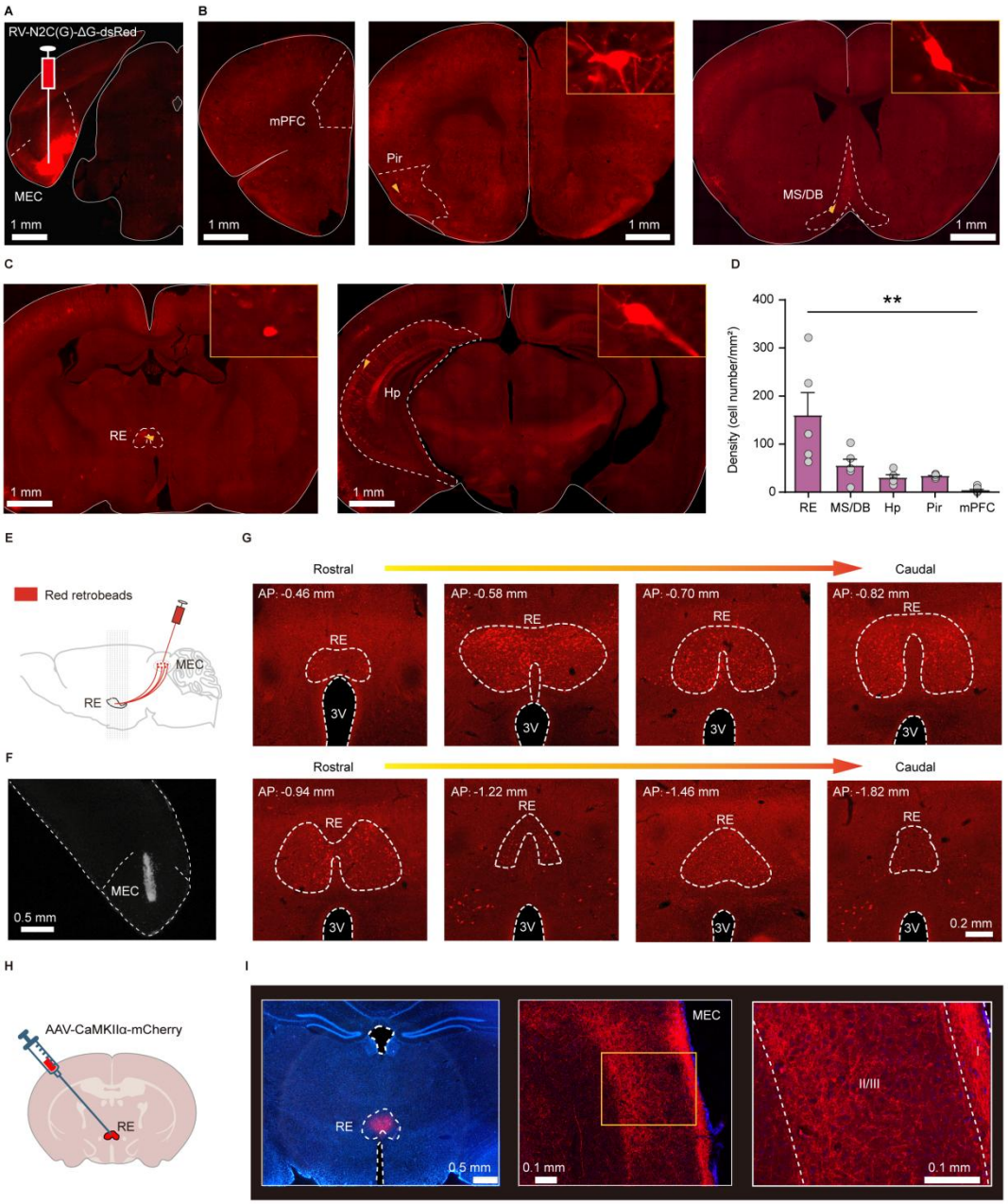

Supplementary Figure 4. MEC receives monosynaptic projections from the RE.

A An example coronal section showing the injection site of RV-N2C(G)-ΔG-dsRed.

B Representative coronal sections showing the expression of RV-dsRed in the medial prefrontal cortex (mPFC), piriform cortex (Pir) and medial septum/digonal band (MS/DB). Inset is the enlarged view of a dsRed-positive neuron expressed in the Pir and MS/DB.

C Same as **B** but for RE and hippocampus (Hp).

D Density of RV-labeled cells distributed in the brain regions identified as the upstream areas of MEC (Kruskal-Wallis One Way Analysis of Variance on Ranks, n = 5 mice for RE, MS/DB, Pir and mPFC, n = 4 mice for Hp, $H = 17.305$, $P = 0.002$. RE vs mPFC: $H = 4.026$, $P = 0.001$).

E Schematic of retrobeads-mediated retrograde tracing.

F Representative image showing the injection site of retrobeads in the MEC.

G Example coronal slices showing the retrobeads labeled neurons in the RE from rostral to caudal. AP: anterior-posterior axis. 3V: third ventricle.

H Schematic showing the mCherry-mediated anterograde tracing from the RE.

I Representative image showing the expression of AAV-CaMKIIα-mCherry in the RE (left). Images showing the expression of mCherry-labeled RE axon terminals in the MEC (middle) and the enlarged view (right).

n = 5 mice were included in the experiment of RV-dsRed mediated retrograde tracing. n = 4 mice were included in the experiment of retrobeads mediated retrograde tracing. $^{**}P < 0.01$. Data are presented as mean ± s.e.m. Source data are provided as a Source Data file.

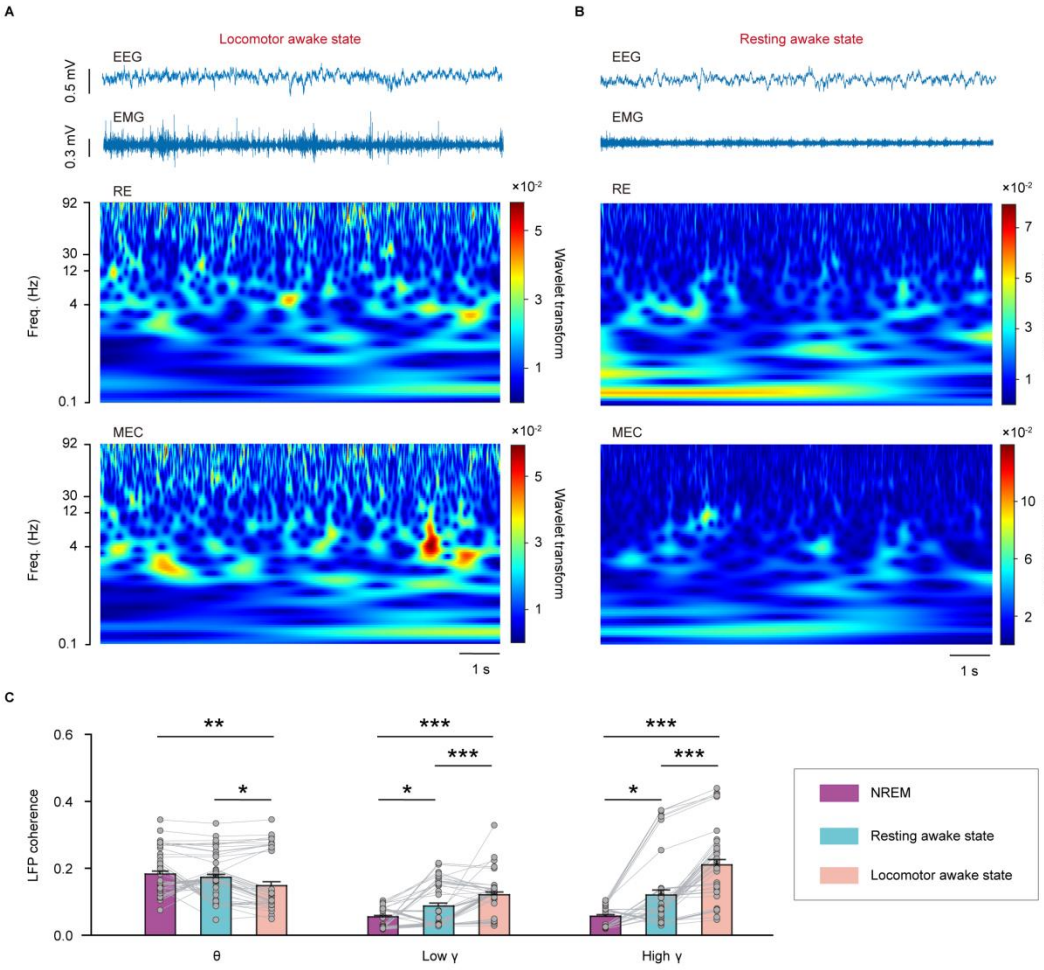

Supplementary Figure 5. LFP coherence between RE and MEC during locomotor awake state, resting awake state and NREM sleep.

A, B Representative raw EEG-EMG traces, LFP in the RE and MEC during locomotor awake state (**A**) and resting awake state (**B**).

C LFP coherence in the RE and MEC during NREM sleep, resting and locomotor awake states (Friedman Repeated Measures ANOVA on Ranks followed by post hoc Student-Newman-Keuls Method, n = 51 channels, theta: $q = 7.569$, $P = 0.023$; low gamma: $q = 20.118$, $P = 4.3\times10^{-5}$; high gamma: $q = 60.118$, $P = 8.82\times10^{-14}$).

$^{*}P < 0.05$, $^{**}P < 0.01$, $^{***}P < 0.001$. Data are presented as mean ± s.e.m. Source data

are provided as a Source Data file.

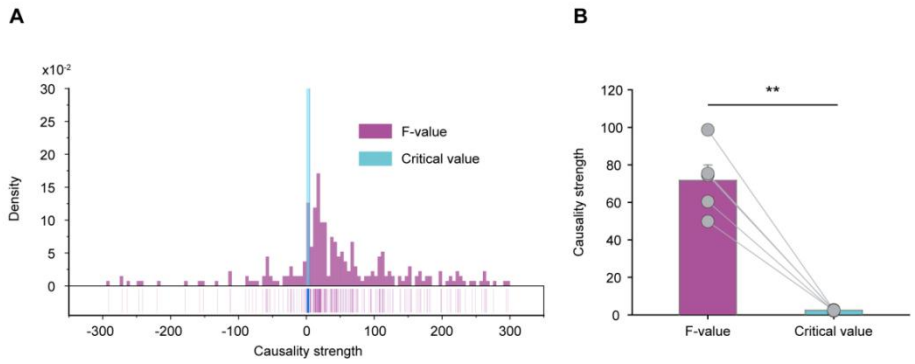

Supplementary Figure 6. Isolated theta waves may propagate from RE to MEC proved by Granger analysis.

A Distribution of the F-value and the critical value calculated by the Granger analysis for the detected theta events.

B Statistical analysis of the calculated F-value and the critical value (Two tailed paired *t* test, n = 5 mice, $t_4 = 8.488$, $P = 0.00106$).

$^{**}P < 0.01$. Data are presented as mean ± s.e.m. Source data are provided as a Source Data file.

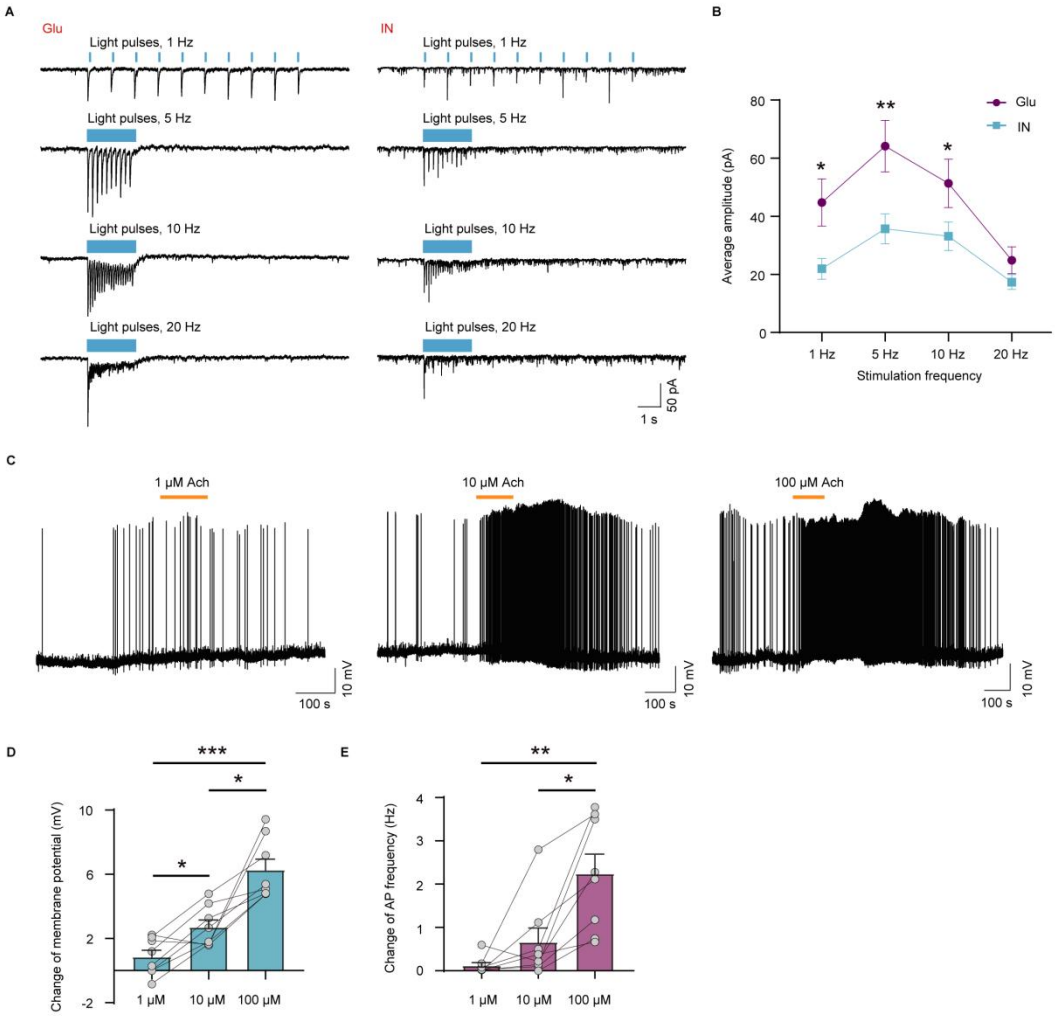

122

123 **Supplementary Figure 7. MEC interneurons are activated by wakefulness-**

124 **promoting neurotransmitter.**

125 **A** Sample voltage-clamp traces showing EPSCs of one example glutamatergic neuron

126 (Glu, left) or GABAergic interneuron (IN, right) evoked by a series of light pulses (1

127 Hz, 5 Hz, 10 Hz, 20 Hz).

128 **B** Average amplitude of EPSCs of MEC glutamatergic neurons (magenta) and

129 GABAergic interneurons (cyan) evoked by a series of light pulses (Scheirer-Ray-Hare

130 test followed by post hoc Holm-Sidak method, Glu: n = 13 cells, IN: n = 13 cells, Glu

131 vs. IN, $H = 3.204$, $P = 3.80\times10^{-5}$; light stimulation frequency factor, $H = 5.681$, $P =$

3.00×10^{-6}; interaction, $H = 0.0271$, $P = 0.647$).

C Representative current-clamp traces of $MEC^{RE\text{-}projecting}$ GABAergic neurons at the baseline and in a bath solution containing 1 µM, 10 µM, 100 µM acetylcholine (Ach).

D, E Change in membrane potential (**D**) and firing frequency (**E**) of $MEC^{RE\text{-}projecting}$ GABAergic neurons in a bath solution containing 1 µM, 10 µM, 100 µM Ach compared with baseline (**D**: One-way Repeated Measures ANOVA followed by post hoc Holm-Sidak method, n = 8 cells, $F_{2,14} = 26.7$, $P = 0.000017$; 1 µM vs. 10 µM: $P = 0.0262$; 1 µM vs. 100 µM: $P = 0.000879$; 10 µM vs. 100 µM: $P = 0.0145$; **E**: One-way Repeated Measures ANOVA followed by post hoc Holm-Sidak method, n = 8 cells, $F_{2,14} = 14.9$, $P = 0.000341$; 1 µM vs. 10 µM: $P = 0.449$; 1 µM vs. 100 µM: $P = 0.006453$; 10 µM vs. 100 µM: $P = 0.0209$).

$^{*}P < 0.05$, $^{**}P < 0.01$, $^{***}P < 0.001$. Data are presented as mean ± s.e.m. Source data are provided as a Source Data file.

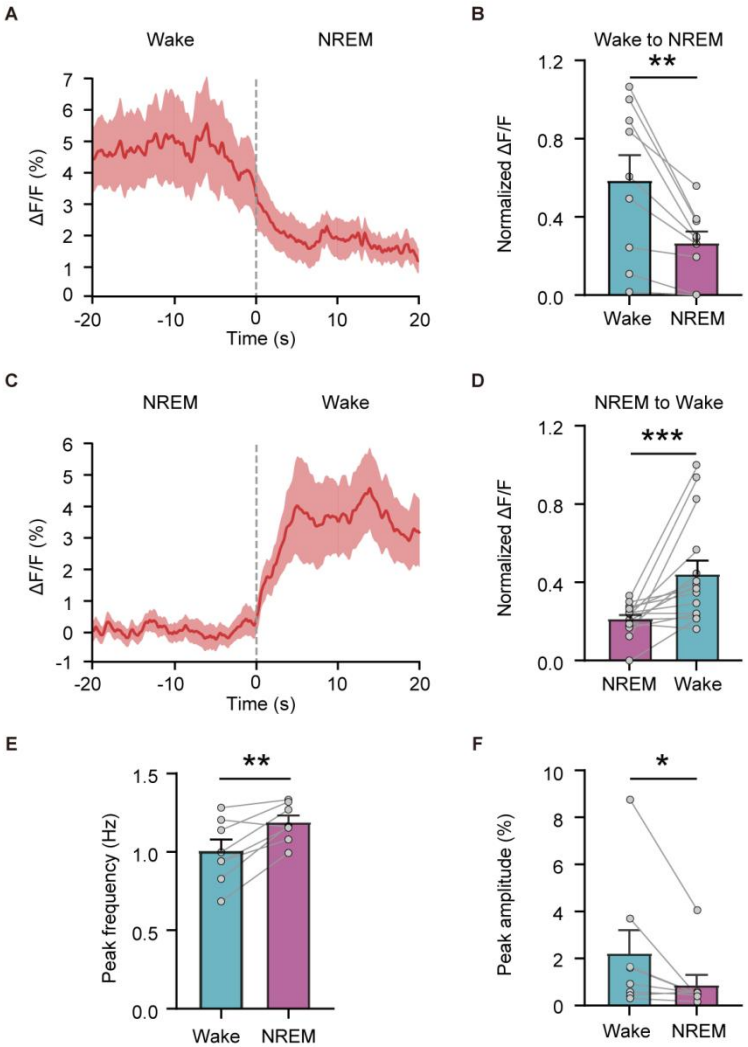

Supplementary Figure 8. Changes in activities of the RE neurons projecting to MEC across sleep-wakefulness cycle.

A, C Ca^{2+} activity of RE neurons projecting to MEC during transitions from wakefulness to NREM sleep (**A**), NREM sleep to wakefulness (**C**). Data are presented as mean (red line) ± s.e.m. (shaded area). Vertical dashed lines indicate the time points of state transitions.

B, D Change in the Ca^{2+} activity before and after state transitions (Wake to NREM: n = 9 trials from 8 mice, two tailed paired *t* test, $t_8 = 3.789$, $P = 0.00532$; NREM to

wake: n = 15 trials from 8 mice, Wilcoxon Signed Rank Test, Z = -3.181, P = 0.00147).

E, F Comparation of Ca^{2+} peak frequency (**E**) and amplitude (**F**) of RE neurons projecting to MEC during wakefulness and NREM sleep (n = 8 mice, Peak frequency: two tailed paired t test, t_7 = -3.929, P = 0.00568; peak amplitude: Wilcoxon Signed Rank Test, Z = -2.100, P = 0.039).

n = 8 mice were included in the experiment of simultaneously recording RE Ca^{2+} activity and MEC LFP (Fig. 4 and Supplementary Figure. 8).

*P < 0.05, **P < 0.01, ***P < 0.001. Data are presented as mean ± s.e.m. Source data are provided as a Source Data file.

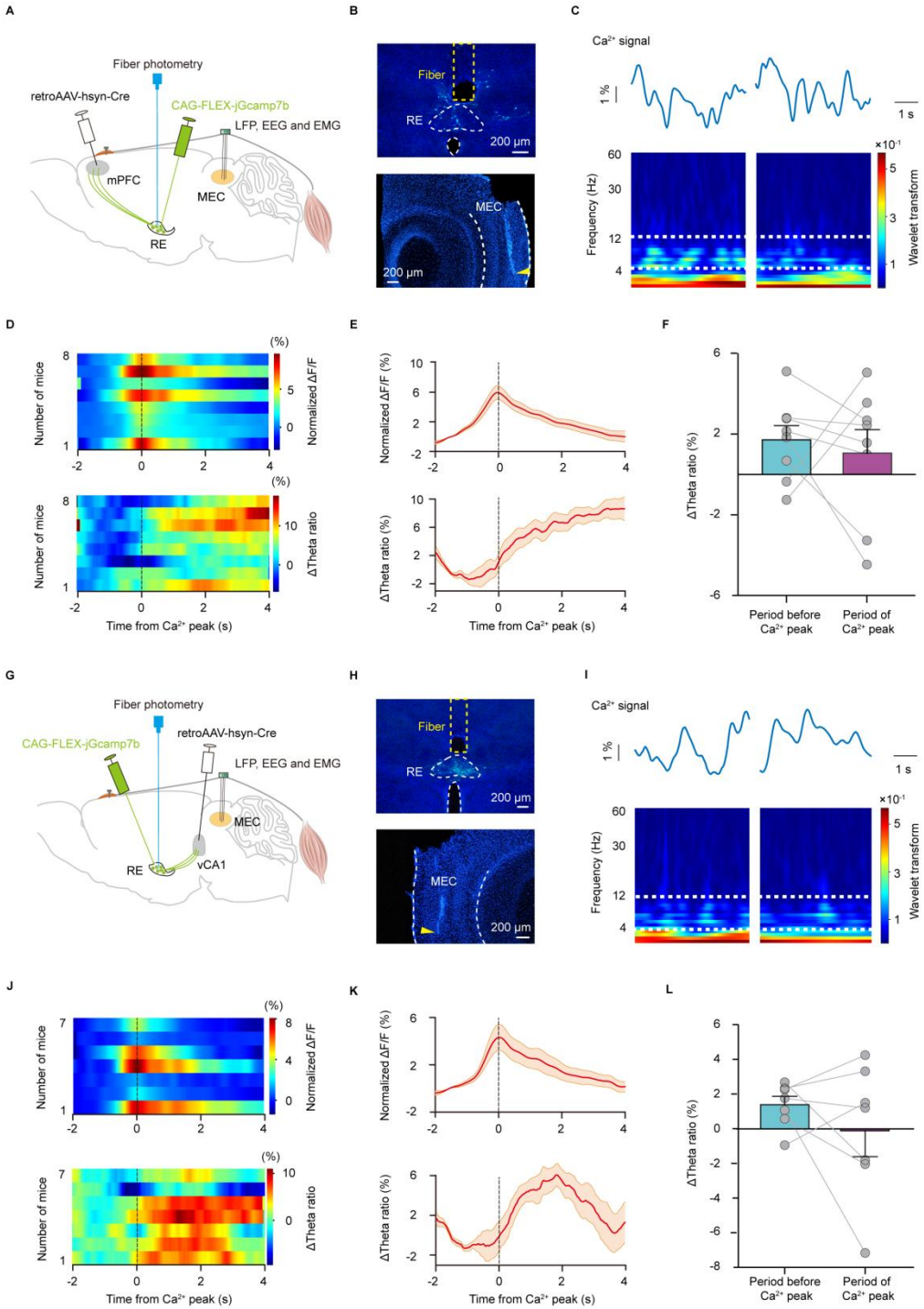

Supplementary Figure 9. MEC theta waves is not positively correlated with the activities of RE neurons projecting to mPFC or vCA1.

A, G Diagram for simultaneously fiber photometry recording of RE neurons projecting to mPFC (**A**) or vCA1 (**G**) as well as LFP recordings in the MEC.

B, H Representative image showing RE neurons projecting to mPFC (**B**) or vCA1 (**H**) expressing jGCaMp7b (green), the optical fiber (dotted yellow pane) implanted in the RE (top), and the electrode implanted in the MEC (bottom, yellow arrowhead).

C, I Synchronous recording of Ca^{2+} activity of RE neurons projecting to mPFC (**C**, top) or vCA1 (**I**, top) and LFP in the MEC (**C** or **I**, bottom) during NREM sleep. Between two dotted white lines is theta frequency band (4-12 Hz).

D, J Heatmaps illustrating the change of Ca^{2+} activity (top) and increment of theta/delta ratio (ΔTheta ratio, bottom) around the peak of Ca^{2+} activity of RE neurons projecting to mPFC (**D**) or vCA1 (**J**) during NREM sleep (n = 8 mice).

E, K Average Ca^{2+} activity and ΔTheta ratio around the peak of Ca^{2+} activity of RE neurons projecting to mPFC (**E**) or vCA1 (**K**) from 8 mice. Data are presented as mean (orange line) ± s.e.m. (shaded area). Vertical dashed lines indicate the time points of Ca^{2+} peak.

F, L ΔTheta ratio before and during the period of Ca^{2+} peak of RE neurons projecting to mPFC (**F**) or vCA1 (**L**) (Two tailed paired *t* test, mPFC: n = 8 mice, $t_7 = 0.458$, $P = 0.661$; vCA1: n = 7 mice, $t_6 = 1.023$, $P = 0.346$).

Data are presented as mean ± s.e.m. Source data are provided as a Source Data file.

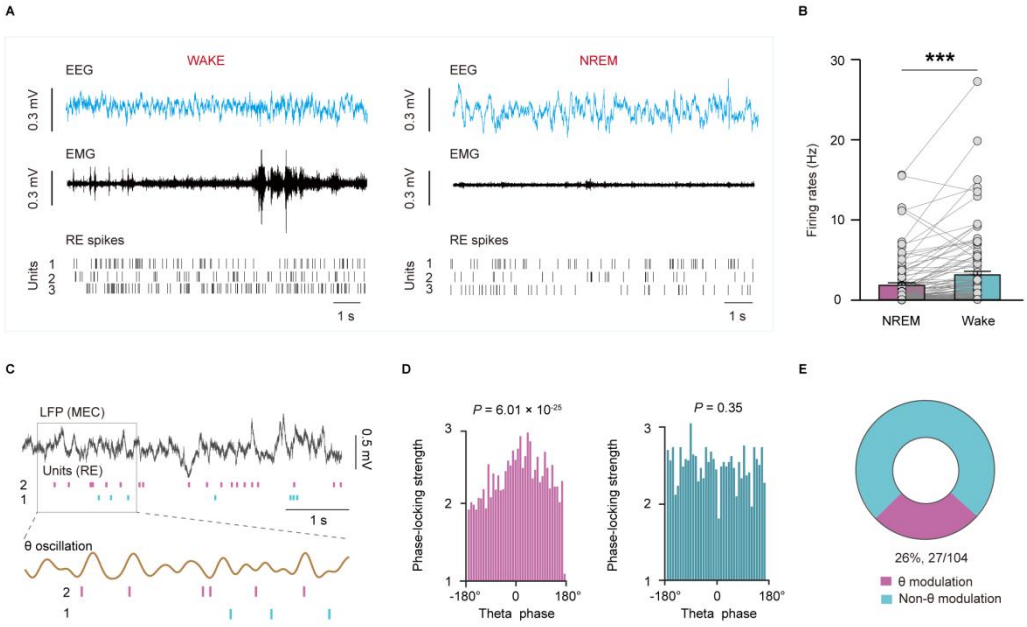

189

190 **Supplementary Figure 10. Spikes recorded in the RE are phase-locked to the**

191 **isolated theta waves in the MEC.**

192 **A** Representative raw EEG-EMG traces, RE spikes during wakefulness (left) and

193 NREM sleep (right).

194 **B** Comparison of RE firing rates during wakefulness and NREM sleep. Each dot

195 represents individual cell (Wilcoxon Signed Rank Test, n = 104 cells, Z = -6.197, P =

196 5.74×10^{-10}).

197 **C** Representative image showing synchronous recording of MEC LFP traces (top) and

198 spikes of two example cells in the RE (bottom). One cell (magenta) exhibited a

199 preference for firing during the up states of MEC theta waves, whereas another cell

200 (cyan) did not demonstrate any theta-phase locking.

201 **D** Phase-locking strength showing units of RE spiking entrained to MEC theta phase.

202 **E** Pie chart showing the percentage of the theta waves-modulated cells and non-theta

modulated cells.

n = 5 mice were included in Fig. 2 and Supplementary Figure. 10.

***P < 0.001. Data are presented as mean ± s.e.m. Source data are provided as a Source Data file.

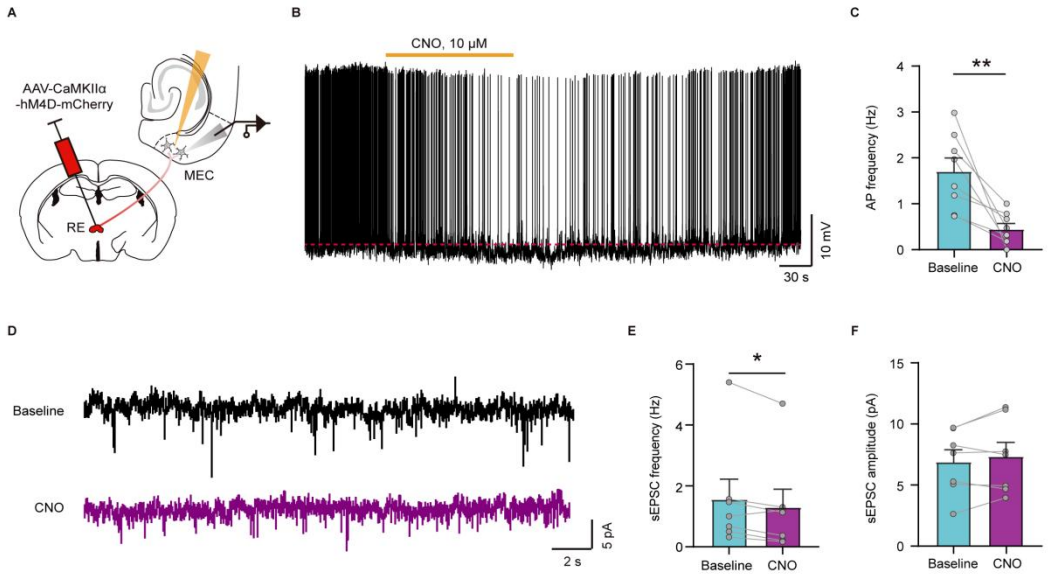

Supplementary Figure 11. Activities of MEC excitatory neurons are down-regulated by chemogenetic inhibition of RE inputs.

A Schematic for investigating the effect of CNO on the activities of MEC neurons.

B Sample traces showing activities of $MEC^{RE\text{-}projecting}$ neurons before, during and after bath application of CNO.

C Change of firing frequency of $MEC^{RE\text{-}projecting}$ neurons during bath application of CNO (Two tailed paired t test, n = 8 cells, $t_7 = 3.812$, $P = 0.00661$).

D Representative traces of spontaneous excitatory postsynaptic currents (sEPSCs) of $MEC^{RE\text{-}projecting}$ neurons at the baseline and in a bath application of CNO.

E, F Change in the sEPSCs frequency (**E**) and amplitude (**F**) of $MEC^{RE\text{-}projecting}$ neurons after bath application of CNO (Two tailed paired *t* test, sEPSCs frequency: n = 7 cells, $t_6 = 2.625$, $P = 0.0393$; sEPSCs amplitude: n = 7 cells, $t_6 = -1.133$, $P = 0.300$).

$^*P < 0.05$, $^{**}P < 0.01$. Data are presented as mean ± s.e.m. Source data are provided as a Source Data file.

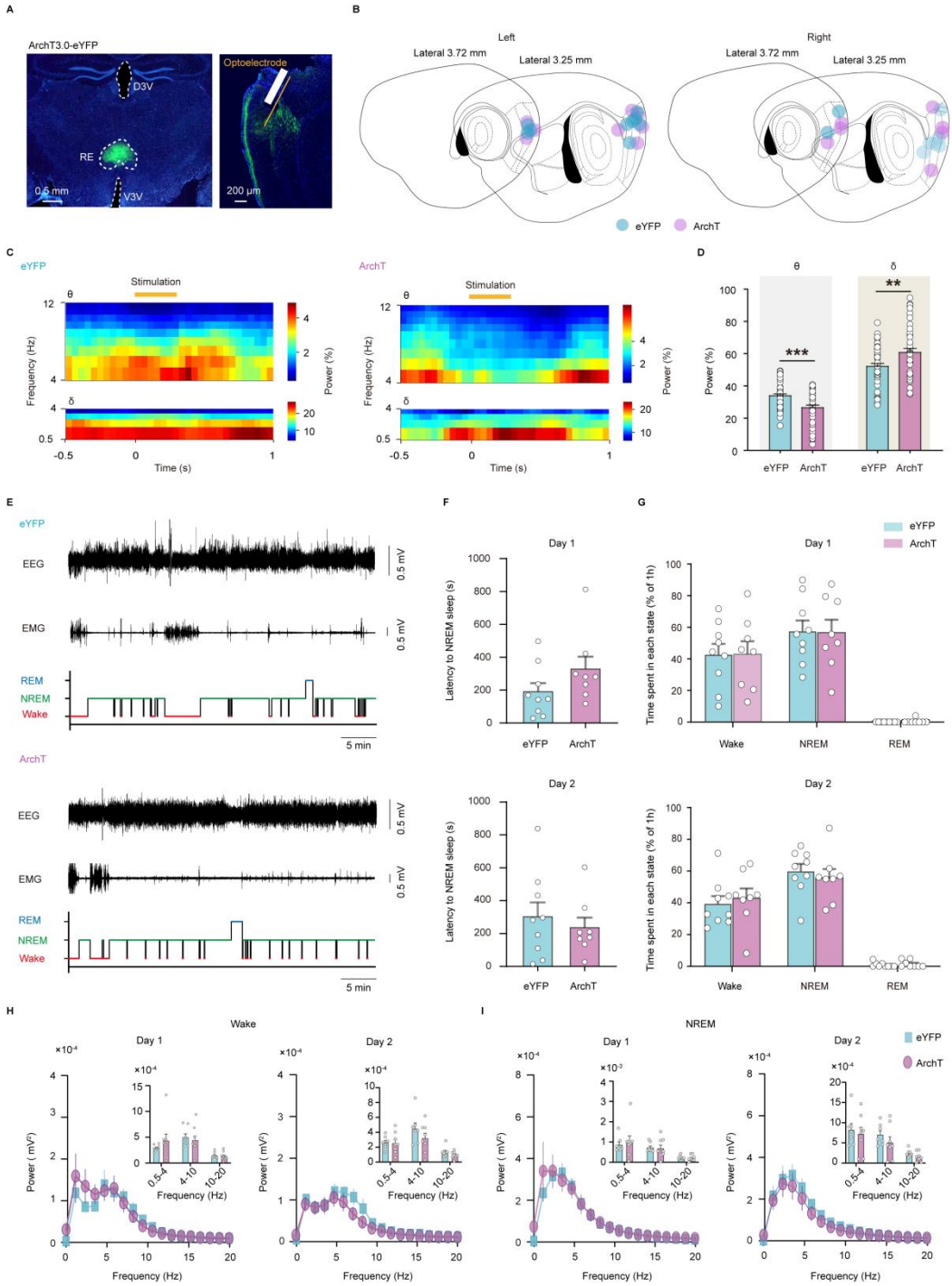

225

226 **Supplementary Figure 12. Closed-loop optogenetic inhibition of RE-MEC**

227 **pathway reduced theta power with sleep-wakefulness architecture unaffected.**

228 **A** Representative image showing the expression of AAV2/9-ArchT3.0-eYFP in the

229 RE (left), the optoelectrode in the MEC (right).

230 **B** Implanted optical fibers were depicted as filled cyan (eYFP, n = 9 mice) or magenta

(ArchT, n = 8 mice) circles for all the tested mice.

C Representative LFP power spectrum of theta and delta frequency around yellow light stimulation delivered during post-training NREM sleep in the eYFP and ArchT group.

D Optogenetic inhibition of RE-MEC pathway reduced theta power, while increased delta power during post-training NREM sleep (eYFP: n = 44 cells, ArchT: n = 42 cells, Two tailed unpaired *t* test, theta power: $t_{84} = 3.741$, $P = 0.000334$; delta power: $t_{84} = -2.763$, $P = 0.00703$).

E Representative raw EEG-EMG traces, and color-coded hypnogram from the mouse of the eYFP (top) or ArchT group (bottom).

F Latency to NREM sleep episodes after training during day 1 and day 2. (eYFP: n = 9 mice, ArchT: n = 8 mice, Day 1: Mann-Whitney Rank Sum Test, $U = 19$, $P = 0.112$, day 2: two tailed unpaired *t* test, $t_{15} = 0.607$, $P = 0.553$).

G Time spent in each state after training during day 1 and day 2 (eYFP: n = 9 mice, ArchT: n = 8 mice, Two tailed unpaired *t* test or Mann-Whitney Rank Sum Test, Day 1-wake: $t_{15} = -0.0331$, $P = 0.974$, day 1-NREM: $t_{15} = 0.0801$, $P = 0.937$; day 1-REM: $U = 31.5$, $P = 0.346$, day 2-wake: $t_{15} = -0.454$, $P = 0.657$; day 2-NREM: $t_{15} = 0.565$, $P = 0.581$; day 2-REM: $U = 31$, $P = 0.612$).

H EEG power density of wakefulness in the eYFP and ArchT group during post-training one hour on day 1 and day 2. Inset is a quantitative analysis of the power in different frequency bands (eYFP: n = 7 mice, ArchT: n = 8 mice, Mann-Whitney Rank Sum Test or two tailed unpaired *t* test. Day 1: 0.5-4 Hz, $U = 19$, $P = 0.336$; 4-10

Hz, t_{13} = 0.442, P = 0.666; 10-20 Hz, t_{13} = 0.404, P = 0.693. Day 2: 0.5-4 Hz, t_{13} = 0.139, P = 0.892; 4-10 Hz, t_{13} = 1.233, P = 0.239; 10-20 Hz, t_{13} = 1.307, P = 0.214).

I Same as **H** but for NREM sleep (Mann-Whitney Rank Sum Test or two tailed unpaired t test. Day 1: 0.5-4 Hz, U = 24, P = 0.694; 4-10 Hz, t_{13} = 0.201, P = 0.844; 10-20 Hz, t_{13} = 0.548, P = 0.593. Day 2: 0.5-4 Hz, t_{13} = 0.428, P = 0.675; 4-10 Hz: t_{13} = 1.073, P = 0.303; 10-20 Hz: t_{13} = 1.600, P = 0.134).

n = 9 mice and 8 mice were included in the eYFP or ArchT group for Fig. 6 and Supplementary Figure. 12.

$^{**}P < 0.01$, $^{***}P < 0.001$. Data are presented as mean ± s.e.m. Source data are provided as a Source Data file.

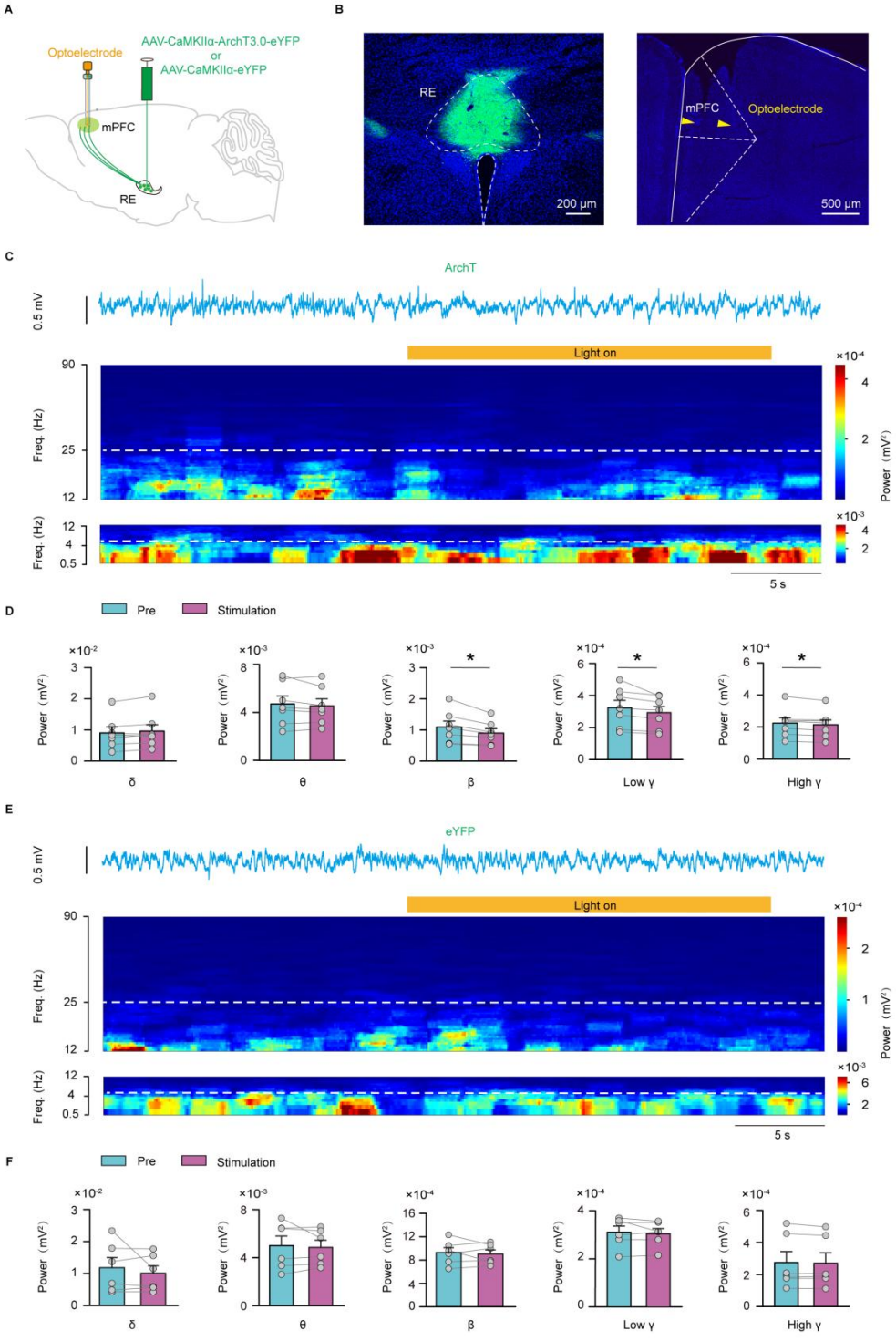

264

265 **Supplementary Figure 13. Effects of optogenetic inhibition of RE-mPFC**

266 **pathway on mPFC network oscillations during NREM sleep.**

267 **A** Schematic of optogenetic inhibition of the RE-mPFC pathway.

B Representative image showing the expression of ArchT-eYFP in the RE (left) and the optoelectrode implanted in the mPFC (yellow arrow, right).

C, E Raw trace of LFP (top) recorded in the mPFC and corresponding power spectrum (bottom) before and during yellow light stimulation during NREM sleep in ArchT (**C**) or eYFP (**E**) group.

D, F Changes in the mPFC LFP after inhibition RE-mPFC pathway during NREM sleep of the ArchT (**D**) or eYFP (**F**) group (ArchT group: n = 7 mice, two tailed paired *t* test or Wilcoxon Signed Rank Test. Delta: t_6 = -2.026, P = 0.0891; theta: t_6 = 1.026, P = 0.345; beta: t_6 = 3.496, P = 0.0129; low gamma: Z = -2.366, P = 0.016; high gamma: t_6 = 3.475, P = 0.0132, eYFP group: n = 6 mice, two tailed paired *t* test or Wilcoxon Signed Rank Test. Delta: Z = -0.314, P = 0.844; theta: Z = 0.105, P = 1.000; beta: t_5 = 0.485, P = 0.648; low gamma: t_5 = 0.731, P = 0.498; high gamma: t_5 = 0.954, P = 0.384).

*P < 0.05. Data are presented as mean ± s.e.m. Source data are provided as a Source Data file.

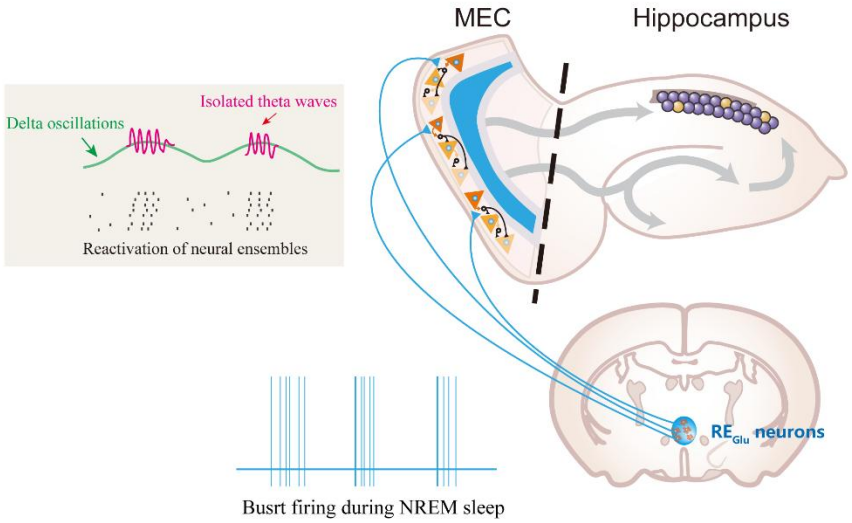

Supplementary Figure 14. A summary schematic illustrates that the midline thalamus drives the isolated theta waves in the MEC, which are essential for memory reactivation during NREM sleep.